Optics Letters

Scaling law of Purcell factor in hyperbolic metamaterial cavities with dipole excitation

Wei Wang, Xiaodong Yang, and Jie Gao*

Department of Mechanical and Aerospace Engineering, Missouri University of Science and Technology, Rolla, Missouri 65409, USA
**Corresponding author: gaojie@mst.edu*

Received 2 October 2018; revised 16 December 2018; accepted 16 December 2018; posted 17 December 2018 (Doc. ID 346998); published 16 January 2019

To control the spontaneous emission rate of dipole emitters, a resonant cavity is widely used to provide large electromagnetic mode confinement, thus resulting in the enhanced Purcell effect. Here, hyperbolic metamaterial cavities with different wavevectors are designed to have identical fundamental mode at the same resonant frequency. The anomalous power law for the Purcell factor of the cavity wavevector is investigated with dipole excitation. Different from conventional photonic and plasmonic cavities, a fifth power law PF$\sim(k/k_0)^5$ for small wavevectors and a square law PF$\sim(k/k_0)^2$ for large wavevectors are demonstrated. The unique optical properties and Purcell factor scaling law of hyperbolic metamaterial cavities will greatly benefit applications in cavity electrodynamics, quantum optics, single photon sources, on-chip quantum computing, and circuits.

https://doi.org/10.1364/OL.44.000471

Control of spontaneous emission of emitters such as quantum dots [1–3], molecules [4], color centers [5], etc., plays an important role in the study of non-classical light emission, fluorescence detection, quantum optics, and quantum information processing [6–12]. According to the Purcell effect [13], spontaneous emission rates of single emitters can be modified by photonic and plasmonic cavities [14–16], which possess both high quality factors and small electromagnetic mode volumes. Recently, hyperbolic metamaterials have drawn a lot of attention due to the large photonic density of states supported in the metamaterials [17–22]. In addition, hyperbolic metamaterial cavities in infrared frequencies have been realized to offer ultrahigh mode refractive indices and small mode volumes [23–25]. Quite different from previously studied photonic and plasmonic cavities, one unique optical property of hyperbolic metamaterial cavities is that along the hyperbolic dispersion curve, a series of nano-cavities with different resonating wavevectors k can be designed to have the same resonant frequency. It provides us an opportunity to study the scaling law for the Purcell factor of the resonance wavevector at a fixed resonant frequency of the cavities (i.e., the emission frequency of the emitters).

In this Letter, we have numerically investigated the scaling law of Purcell factors for dipole emitters coupled with hyperbolic metamaterial cavities. A series of 12 Au-Al_2O_3 multilayer nano-cavities with different sizes is designed with fundamental electromagnetic mode at 850 nm with the finite element method (FEM). The resonating wavevector, mode area, quality factor, and Purcell factor are calculated for each cavity. Purcell factors for different dipole positions and orientations have also been studied. Most importantly, anomalous power law for the Purcell factor of the cavity wavevector has been demonstrated. This scaling law result provides a new aspect for investigating Purcell factors in hyperbolic metamaterial cavities, contrary to conventional optical cavities. The current study is also of great interest in fundamental research fields such as cavity electrodynamics and quantum optics, as well as a variety of applications such as single photon sources, on-chip quantum computing, and circuits.

Hyperbolic multilayer nano-cavity design: a schematic of a two-dimensional (2D) hyperbolic multilayer nano-cavity is shown in Fig. 1(a), where the multilayer consists of alternative 4 nm Au and 6 nm Al_2O_3 layers (40% fill ratio of gold). The permittivity of Au is described by the Drude model $\varepsilon_m = \varepsilon_\infty - \omega_p^2/(\omega^2 + i\omega\gamma)$, with permittivity constant $\varepsilon_\infty = 1$, plasma frequency $\omega_p = 1.37 \times 10^{16}$ rad/s, and damping factor $\gamma = 4.08 \times 10^{13}$ rad/s. The dielectric constant of Al_2O_3 is $\varepsilon_d = 2.28$. The multilayer metamaterial permittivity can be described using the effective media theory (EMT) [19] with a uniaxial dielectric tensor $\overleftrightarrow{\varepsilon}(\vec{r}) = \mathrm{diag}(\varepsilon_{xx}, \varepsilon_{yy}, \varepsilon_{zz})$ [15,26], where $\varepsilon_{xx} = \varepsilon_{yy} = p\varepsilon_m + (1-p)\varepsilon_d$, $\varepsilon_{zz} = \varepsilon_m\varepsilon_d/[(1-p)\varepsilon_m + p\varepsilon_d]$, p is the fill radio of metal, and ε_m and ε_d are the permittivities of metal and dielectric, respectively. When the extraordinary (TM-polarized) wave propagates in strongly anisotropic metamaterial, the iso-frequency contour (IFC) can be drawn according to the following equation [17]:

$$\frac{k_x^2}{\varepsilon_\perp} + \frac{k_z^2}{\varepsilon_\parallel} = \frac{\omega^2}{c^2}. \tag{1}$$

Within the interested wavelength range of a typical quantum dot dipole emitter, e.g., at 850 nm, the real parts of the permittivity principal components of the multilayer metamaterials have opposite signs, which leads to the hyperbolic IFC as shown in Fig. 1(b) (white lines). For multilayers with finite

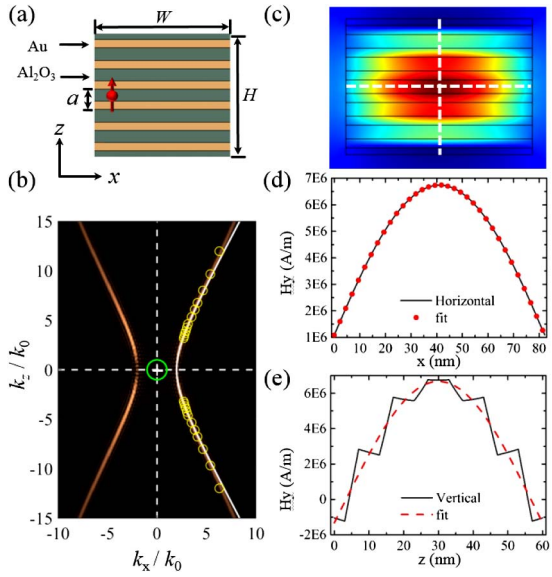

Fig. 1. (a) Schematic of 2D multilayer nano-cavity made of alternate Au (4 nm) and Al_2O_3 (6 nm). Period of the multilayer is denoted by *a*, and dipole emitter is illustrated by the red dot. (b) IFC for multilayer metamaterials calculated from FFT (bronze colored lines) and EMT (white lines) at wavelength of 850 nm. The yellow circles represent the extracted resonating wavevectors of the designed cavity modes, and the green circle represents the light cone of vacuum. (c) Eigenmode magnetic field distribution for cavity with size (82.2 nm × 60 nm). (d), (e) Magnetic field profiles along the horizontal and vertical middle lines of eigenmode are fitted to extract the wavevectors inside each cavity.

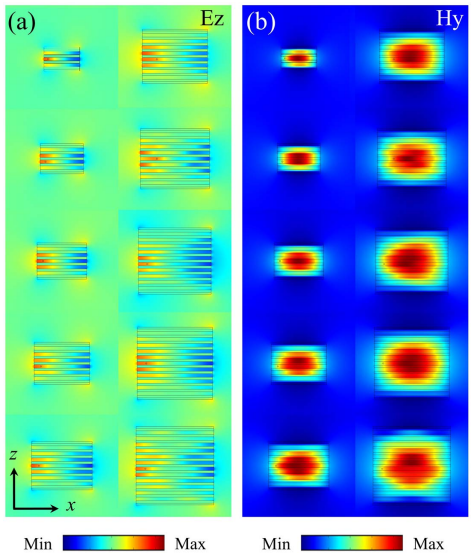

Fig. 2. Fundamental electric (a) and magnetic (b) modes excited by an electric dipole placed inside each cavity with cavity height H from 40 nm to 130 nm. The electric dipole is positioned at the middle dielectric layer where the electric field is the maximum. All cavities are resonating with fundamental mode order (1, 1) at 850 nm.

layer thicknesses, optical nonlocality leads to the effective permittivity tensor that is related not only to the frequency but also to the wavevector [27]. The IFC considered the nonlocal effect can be obtained by spatial Fourier analysis (FFT) of the electric field excited by a dipole emitter placed inside the multilayer [28], shown as bronze colored lines in Fig. 1(b). In the low k region ($k \ll 2\pi/a$), the IFC calculated from EMT matches with the Fourier analysis. In the high k region where the wavelength gets close to the period of the multilayers, the dispersion curve deviates from the effective medium calculation at the edge of the first Brillouin zone [23,28]. Metamaterials with hyperbolic IFCs can support very large wavevectors and optical density of states, which will strongly enhance light–matter interaction such as spontaneous emission [17,19]. Furthermore, nano-cavities can be designed based on hyperbolic multilayer metamaterials with extreme large refractive indices and ultrasmall mode volumes [28]. As illustrated in Fig. 2(a), a series of 2D nano-cavities consisting of 4 to 13 pairs of Au-Al_2O_3 layers (corresponding to cavity height H from 40 nm to 130 nm) is designed with identical fundamental resonances at 850 nm. The top and bottom layer is set to Al_2O_3 with half the normal dielectric layer thickness as 3 nm to protect the Au layer. The cavity width W can be approximately expressed as $W \approx 2\pi/\sqrt{|\varepsilon_\perp|(\omega^2/c^2 - \pi^2/(|\varepsilon_\parallel|H^2))}$ according to the EMT and dispersion relation [29]. Further tunings of the cavity widths are performed in the eigen-frequency analysis with the approximated W values as the initial design parameter, and the final geometric dimensions of the nano-cavities are optimized in order to ensure that a series of nano-cavities of different sizes supports fundamental resonant mode at 850 nm. For example, as shown in Fig. 1(c), eigen-frequency analysis gives the width design of 82.2 nm for a cavity with height of 60 nm, and the magnetic field distribution of the fundamental eigenmode is presented. Wavevectors kx and kz of the cavity mode can be extracted by fitting the magnetic field profiles along the middle cut lines in Fig. 1(c) with $H_y(x,z) = A_1 \cos(k_x x + \varphi_1) A_2 \cos(k_z z + \varphi_2)$, as shown in Figs. 1(d)–1(e). Yellow circles in Fig. 1(b) mark all the extracted wavevectors for all the designed cavities, which coincide with the multilayer hyperbolic IFC very well.

Scaling law of Purcell factor: the Purcell effect is the enhancement of a quantum emitter's spontaneous emission rate by its environment [14]. The Purcell factor (PF) defined as the ratio between the modified spontaneous emission rate γ_{SE} in nanostructures and free-space γ_0 can be obtained by [30]

$$\mathrm{PF} = 1 - \eta + \eta(P/P_0) \quad \textbf{(2)}$$

in full-wave electromagnetic simulation, where $P(P_0)$ is total emission power from the dipole emitter including both the radiated and dissipated power in nanostructures (free space) calculated by integrating the power flow through the boundaries, and η is internal quantum efficiency (we set it to unity for our calculation) [17,19]. In order to investigate the scaling law for Purcell factors of wavevectors, for each designed nano-cavity, an electric dipole emitter with dipole moment along z direction is placed inside the cavity, and total dipole emission power is calculated with FEM simulation. The position of the dipole is chosen to be in the middle dielectric layer where the maximum of electric field locates, as illustrated in Fig. 1(a). Under dipole excitation, identical fundamental modes have been excited at 850 nm as confirmed by the electric field and magnetic field distributions of each cavity presented in Fig. 2. Taking the ratio of total emission power from the dipole inside the nano-cavity

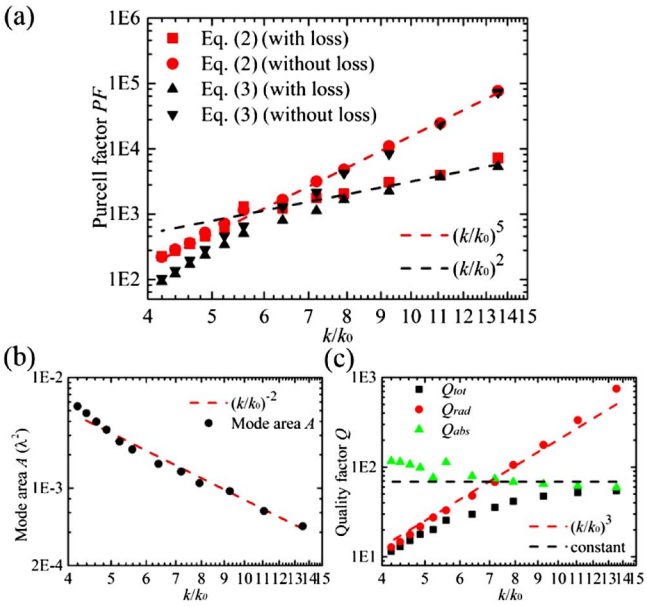

Fig. 3. (a) Purcell factors of hyperbolic metamaterial nano-cavities as a function of k/k_0. The red square and dot represent the Purcell factors calculated by total emission power with and without metal loss. The black up- and down-pointing triangles represent the Purcell factors calculated by Eq. (3). (b) Mode area as a function of wavevector. (c) Red dots represent Q_{rad} with the unique scaling law of $Q_{rad} \sim (k/k_0)^3$. Black squares and green triangles represent Q_{tot} and Q_{abs}, respectively.

and in free space, Purcell factors as a function of the resonating wavevectors of a 2D cavity mode are plotted in Fig. 3(a), where the red circle and square represent the cases with ideal lossless metal and realistic lossy metal, respectively. We can observe that a clear fifth power scaling law of PF $\sim (k/k_0)^5$ can be seen in the log–log plot (red dashed line) for the lossless case. When metal loss is considered, the Purcell factor scaling law still follows the fifth power for small wavevectors; however, PF $\sim (k/k_0)^2$ is presented for large wavevectors, shown as the black dashed line. The results reveal that for hyperbolic metamaterial nano-cavities that support very large wavevectors and high mode indices, Purcell factors grow rapidly and follow distinct scaling laws in the large and small wavevector regions.

In order to further understand the underlying physics of the scaling law and compare to the case of conventional optical cavities, quality factors and mode areas of hyperbolic metamaterial 2D nano-cavities are investigated as a function of resonating wavevectors, and Purcell factors can be evaluated by the following equation [14]:

$$\mathrm{PF} = \frac{1}{\pi^2}\left(\frac{\lambda}{n}\right)^2 \frac{Q}{A}\left(\frac{|E|}{|E_{\max}|}\cos\theta\right)^2, \tag{3}$$

where n is the effective refraction index, λ is wavelength in vacuum, Q is the cavity quality factor, A is the cavity mode area, E is the electric field at the position of the emitter, and θ is the angle between the dipole moment and the local electric field. The mode area A is defined as the ratio of electromagnetic energy in the entire space over the maximum electromagnetic energy density [26,31], $A = [\int \varepsilon(\vec{r})|\vec{E}(\vec{r})|^2 \mathrm{d}^2\vec{r}]/\max[\varepsilon(\vec{r})|\vec{E}(\vec{r})|^2]$. As shown in Fig. 2(a), most of the electromagnetic energy is confined inside the cavity due to the extremely high refractive mode index, but the cavity corners still scatter high k waves and result in radiation energy loss. Total energy in the entire space is integrated across all the simulation area (~1.5 μm × 1.5 μm), which is large enough compared to the cavity size and sufficient to include all the electromagnetic energy. The maximum energy density is found in the middle dielectric layer where the electric dipole is also placed. Figure 3(b) shows the relation between mode area and wavevector for all cavities in a log–log plot. The scaling law of $A \sim (k/k_0)^{-2}$ (red dashed line) is shown. The relationship between mode volume and wavevector in a 3D situation will follow a power law of $(k/k_0)^{-3}$ as expected [32].

To examine the quality factor of each designed nano-cavity, the emission spectrum from an electric dipole from 750 nm to 1000 nm is obtained and fitted with the Lorentzian function [28]. The total quality factor is calculated by $Q_{tot} = \omega/\Delta\omega$, where ω is the cavity resonance frequency, and $\Delta\omega$ is the full width at half maximum of the spectrum. As shown in Fig. 3(c), Q_{tot} gradually increases and approaches a constant of ~70 with the increase of wavevector. Both radiation and absorption contribute to the total quality factor $1/Q_{tot} = 1/Q_{rad} + 1/Q_{abs}$; however, Q_{rad} dominates when there is no metal loss, while Q_{abs} determines the upper bound when realistic metal loss and absorption are considered. Green triangles in Fig. 3(c) depict that Q_{abs} is almost a constant and is independent of the wavevector, since absorption is strongly related to the material loss rather than cavity geometry. However, contrary to conventional 2D cavities, Q_{rad} scales inversely with the cavity size and is proportional to the wavevector following a third power law, giving $Q_{rad} \sim (k/k_0)^3$, as the red dashed line shows. This is because a larger refractive mode index is supported, and less radiation energy leaks out of the cavity with increasing wavevectors for hyperbolic metamaterial nano-cavities [23]. This relationship can also be understood as $Q_{rad} \sim n/\alpha_{rad}$, where α_{rad} is radiation loss due to total internal reflection, which is proportional to $(k/k_0)^{-2}$ in two dimensions, and n is proportional to k/k_0, so Q_{rad} is linearly proportional to $(k/k_0)^3$ [14,28]. Thus, at small wavevectors, Q_{tot} follows the $(k/k_0)^3$ scaling law as Q_{rad}, and gradually approaches Q_{abs} when k/k_0 increase.

Purcell factors can be obtained by Eq. (3) with the calculated quality factor and mode area, showing as the black up- and down-pointing triangles in Fig. 3(a). When the size of the cavity decreases and the corresponding wavevector increases, the mode area of each cavity decreases but the quality factor increases, which leads to the increase in Purcell factor. Without metal loss, a universal fifth power law PF $\sim (k/k_0)^5$ for the Purcell factor of the wavevector is demonstrated, agreeing very well with the emission power ratio calculation. When metal loss and absorption are considered, at small wavevectors, the Purcell factor scaling law follows a fifth power law because radiation dominates the quality factor in this regime, while at large wavevectors, the scaling law follows a square law PF $\sim (k/k_0)^2$, as the black dashed line indicates. The reason is that a huge moment mismatch between the cavity and free space reduces radiation loss, and the absorption dominates the quality factor in the high k regime. As a result, most of the Purcell-effect-enhanced total dipole emission power radiates out from the cavity into the far field in the small k regime but dissipates inside the cavity in the high k regime. Although the simulation is carried out in 2D, the relationship between

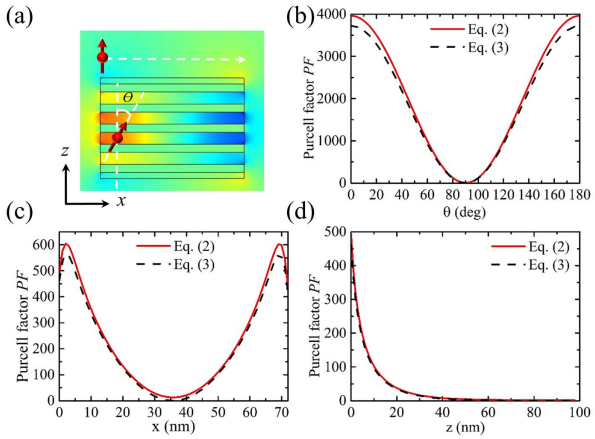

Fig. 4. (a) Schematic of differnet dipole positions and orientations when it is coupled to the hyperbolic multilayer nano-cavity with size (71.6 nm × 50 nm). (b) Dependece of Purcell factor on the dipole orientation, where θ is the angle between the dipole moment and the local electric field vector. $\theta = 0°/180°$ (90°) represents dipole moment along $z(x)$ direction. (c), (d). Calculated Purcell factor for dipole positions on top of the nanocavity moving along x/z directions (indicated by the white dashed lines).

Purcell factor and wavevector in 3D will follow a seventh power law with small wavevectors ($Q_{\text{rad}} \sim n/\alpha_{\text{rad}} \sim (k/k_0)^4$ and $V \sim (k/k_0)^{-3}$) and approach a third power law with large wavevectors, as predicated from the 2D results.

Furthermore, the dependences of Purcell factors on the dipole positions and moment orientations are investigated to reveal the possible experimental situations when quantum dots couple to the nano-cavities with random orientations and at various positions, as shown in Fig. 4(a). Figure 4(b) shows that the Purcell factor reaches maximum when the dipole locates at the electric field maximum and the dipole moment is aligned parallel to the electric field Ez, and decreases when the dipole moment rotates due to the inefficient coupling to the cavity mode. Figures 4(c) and 4(d) show the Purcell factor drops when the dipole is placed on top of the nano-cavity and vanishes when the dipole moves along the x/z direction to the locations where electromagnetic fields are very weak. The calculated Purcell factors from the emission power ratio agree very well with the Cos function and electric field distribution terms, explicitly shown in Eq. (3).

In conclusion, the anomalous power law for the Purcell factors has been demonstrated for hyperbolic metamaterial cavities with dipole excitation. Contrary to conventional optical cavities, identical fundamental resonance mode is supported in a series of hyperbolic multilayer nano-cavities with different resonating wavevectors. A fifth power law PF $\sim (k/k_0)^5$ for small wavevectors and a square law PF $\sim (k/k_0)^2$ for large wavevectors have been shown for 2D hyperbolic cavities. The Purcell factors calculated from the emission power ratio can be understood well from the scaling laws for the quality factor and mode area of the cavity mode. The results provide a new aspect for investigating Purcell factors in hyperbolic metamaterial cavities, and could be of great interest for nanophotonic applications including cavity quantum electrodynamics, single photon sources, optical nonlinearities, optomechanics, fluorescence biosensing, and quantum communication.

Funding. National Science Foundation (NSF) (DMR-1552871, ECCS-1653032); Office of Naval Research (ONR) (N00014-16-1-2408).

Acknowledgment. We thank Qian Wang for the helpful discussion.

REFERENCES

1. A. P. Alivisatos, Science **271**, 933 (1996).
2. Y. Liang, J.-S. Moon, R. Mu, and J. G. Winiarz, J. Mater. Chem. C **3**, 4134 (2015).
3. J.-S. Moon, Y. Liang, I. Kim, J.-W. Oh, and J. G. Winiarz, Polym. Bull. **73**, 2463 (2016).
4. M. D. Eisaman, J. Fan, A. Migdall, and S. V. Polyakov, Rev. Sci. Instrum. **82**, 071101 (2011).
5. M. Y. Shalaginov, V. V. Vorobyov, J. Liu, M. Ferrera, A. V. Akimov, A. Lagutchev, A. N. Smolyaninov, V. V. Klimov, J. Irudayaraj, and A. V. Kildishev, Laser Photon. Rev. **9**, 120 (2015).
6. S. Castelletto and R. Scholten, Eur. Phys. J. **41**, 181 (2008).
7. Y. Liang, W. Wang, J.-S. Moon, and J. G. Winiarz, Opt. Mater. **58**, 203 (2016).
8. M. Toishi, D. Englund, A. Faraon, and J. Vučković, Opt. Express **17**, 14618 (2009).
9. X. R. Jin and J. Gao, Opt. Lett. **38**, 2110 (2013).
10. X. R. Jin, L. Sun, X. Yang, and J. Gao, Opt. Lett. **38**, 4078 (2013).
11. V. Flauraud, R. Regmi, P. M. Winkler, D. T. Alexander, H. Rigneault, N. F. Van Hulst, M. F. García-Parajo, J. R. M. Wenger, and J. R. Brugger, Nano Lett. **17**, 1703 (2017).
12. J.-S. Moon, Y. Liang, T. E. Stevens, T. C. Monson, D. L. Huber, B. D. Mahala, and J. G. Winiarz, J. Phys. Chem. C **119**, 13827 (2015).
13. E. M. Purcell, H. C. Torrey, and R. V. Pound, Phys. Rev. **69**, 37 (1946).
14. D. Englund, D. Fattal, E. Waks, G. Solomon, B. Zhang, T. Nakaoka, Y. Arakawa, Y. Yamamoto, and J. Vučković, Phys. Rev. Lett. **95**, 013904 (2005).
15. C. Guclu, T. S. Luk, G. T. Wang, and F. Capolino, Appl. Phys. Lett. **105**, 123101 (2014).
16. D. Lu, J. J. Kan, E. E. Fullerton, and Z. Liu, Nat. Nanotechnol. **9**, 48 (2014).
17. H. N. Krishnamoorthy, Z. Jacob, E. Narimanov, I. Kretzschmar, and V. M. Menon, Science **336**, 205 (2012).
18. A. Chebykin, A. Orlov, A. Shalin, A. Poddubny, and P. Belov, Phys. Rev. B **91**, 205126 (2015).
19. L. Li, W. Wang, T. S. Luk, X. Yang, and J. Gao, ACS Photon. **4**, 501 (2017).
20. Z. Li, W. Wang, D. Rosenmann, D. A. Czaplewski, X. Yang, and J. Gao, Opt. Express **24**, 20472 (2016).
21. L. Sun, X. Yang, W. Wang, and J. Gao, J. Opt. **17**, 035101 (2015).
22. W. Wang, D. Rosenmann, D. A. Czaplewski, X. Yang, and J. Gao, Opt. Express **25**, 20454 (2017).
23. J. Yao, X. Yang, X. Yin, G. Bartal, and X. Zhang, Proc. Natl. Acad. Sci. USA **108**, 11327 (2011).
24. L. Ferrari, C. Wu, D. Lepage, X. Zhang, and Z. Liu, Prog. Quantum Electron. **40**, 1 (2015).
25. Y. He, H. Deng, X. Jiao, S. He, J. Gao, and X. Yang, Opt. Lett. **38**, 1179 (2013).
26. A. F. Koenderink, Opt. Lett. **35**, 4208 (2010).
27. A. Chebykin, A. Orlov, A. Vozianova, S. I. Maslovski, Y. S. Kivshar, and P. A. Belov, Phys. Rev. B **84**, 115438 (2011).
28. X. Yang, J. Yao, J. Rho, X. Yin, and X. Zhang, Nat. Photonics **6**, 450 (2012).
29. A. A. Orlov, P. M. Voroshilov, P. A. Belov, and Y. S. Kivshar, Phys. Rev. B **84**, 045424 (2011).
30. B. E. Saleh, M. C. Teich, and B. E. Saleh, *Fundamentals of Photonics* (Wiley, 1991).
31. Z. Li, L. Stan, D. A. Czaplewski, X. Yang, and J. Gao, Opt. Express **26**, 5616 (2018).
32. D. Englund, I. Fushman, and J. Vuckovic, Opt. Express **13**, 5961 (2005).